SENSORS

A skin-inspired tactile sensor for smart prosthetics

Yuanzhao Wu[1,2,3], Yiwei Liu[1,2]*, Youlin Zhou[1,2], Qikui Man[1,2], Chao Hu[1,2], Waqas Asghar[1,2,3], Fali Li[1,2,3], Zhe Yu[1,2,3], Jie Shang[1,2], Gang Liu[1,2], Meiyong Liao[4], Run-Wei Li[1,2]*

Recent achievements in the field of electronic skin have provided promising technology for prosthetic systems. However, the development of a bionic tactile-perception system that exhibits integrated stimuli sensing and neuron-like information-processing functionalities in a low-pressure regime remains a challenge. Here, we demonstrate a tactile sensor for smart prosthetics based on giant magneto-impedance (GMI) material embedded with an air gap. The sensor exhibits a high sensitivity of 120 newton^{-1} (or 4.4 kilopascal^{-1}) and a very low detection limit of 10 micronewtons (or 0.3 pascals). The integration of the tactile sensor with an inductance-capacitance (LC) oscillation circuit enabled direct transduction of force stimuli into digital-frequency signals. The frequency increased with the force stimuli, consistent with the relationship between stimuli and human responses. The minimum loading of 50 micronewtons (or 1.25 pascals), which is less than the sensing threshold value of human skin, was also encoded into the frequency, similar to the pulse waveform of humans. The proposed tactile sensor not only showed desirable sensitivity and low detection limit but also exhibited transduction of digital-frequency signals like human stimuli responses. These features of the GMI-based tactile sensor show potential for its applications in smart prosthetics, especially prosthetic limbs that can functionally replace natural limbs.

INTRODUCTION

Human skin perceives pressure stimuli on touch, which are subsequently transformed into physiological responses; these responses are transferred to the brain via the nervous system (*1*–*4*). The quality of life for persons with limb loss is greatly affected because of lack of tactile sensing capability. To achieve a close-to-natural replacement, it is important to develop a tactile sensory system that perceives stimuli, encodes them into physiological responses, and then delivers them to the nerves or the brain to form sensory feedback (*5*, *6*). Therefore, researchers are motivated to develop sensors for embedded prosthetics and artificial skin that can restore tactile sensation to disabled persons (*1*, *7*–*12*). There has been notable advancement in the field of designing prosthetic limbs integrated with rigid and/or flexible tactile sensors that are responsive to variable environments (*11*). Despite these advancements, prosthetic limbs cannot be fully used as a functional replacement of natural limbs for disabled persons because of signal incompatibility, that is, the digital pulse signals of humans and the analog signals from artificial tactile sensors. In this case, the development of next-generation prosthetic limbs that replace or even surpass the sensing ability of humans is very important. High tactile sensitivity, ultralow pressure detection, and the ability to encode stimuli into action potentials mimicking those of humans are the required parameters for fabrication of high-performance tactile sensors.

High-performance e-skin tactile sensors can be prepared by using flexible piezoresistors (*13*, *14*), capacitors (*15*, *16*), or organic field-effect transistors based on nanomaterials, for example, carbon nanotubes (CNTs) (*17*–*20*), graphene (*21*), metallic nanowires (*22*–*24*), or conductive polymer materials (*25*). Novelty in structure also affects the sensitivity and detection limit of tactile sensors. In particular, polydimethylsiloxane (PDMS) patterned with microstructure has shown promise for the design of a highly sensitive pressure sensor (*13*, *26*–*30*). Park *et al.* (*31*) used a porous PDMS structure and achieved high sensitivity (1.5 kPa^{-1}), whereas Wang *et al.* (*32*) reported a sensor based on a silk microstructured surface that exhibited superior sensitivity (1.80 kPa^{-1}) and a very low detectable pressure limit (0.6 Pa). Miyamoto *et al.* (*33*) reported lightweight and stretchable on-skin electronics with nanomeshes. Saraf *et al.* (*34*) introduced a light-harvesting and self-powered monolith tactile sensor.

To provide a richer and more natural form of feedback, some approaches have been developed to elicit tactile perception (*35*–*37*). For example, Oddo *et al.* (*38*) reported an approach of intraneural stimulation that elicited discrimination of textural features by an artificial fingertip in intact and amputee humans. Osborn *et al.* (*39*) also developed a multilayered electronic dermis, which exhibited properties based on the behavior of mechanoreceptors and nociceptors, to provide neuromorphic tactile information to an amputee. These approaches open new opportunities for sensory restoration in neuroprosthetic hands. If tactile feedback is increasingly biomimetic, then it will become more natural, rich, and meaningful to the patient. The sensory feedback system could be more compatible with humans if the tactile sensor is able to encode stimuli by mimicking action potentials, which convert mechanical stimuli into physiological signals efficiently (Fig. 1A). Therefore, conversion of time-domain signals to frequency-domain signals is the key factor for artificial tactile sensors. Tee *et al.* (*40*) conducted a tactile sensing technology study on live neuron–compatible organic material. In this study, the integration of a CNT-based tactile sensor with organic transistor-based flexible oscillators enabled direct transduction of force stimuli into digital-frequency signals. The output frequency showed a sublinear response to the force stimuli in the range of 10 to ~100 kPa. This work represents a step toward the design and use of an e-skin with neural-integrated touch feedback mechanism for replacement of limbs. Kim *et al.* (*41*) developed neuromorphic technology in neuroprosthetics. The spikes emitted by the proposed artificial tactile sensor (neural afferent) were directly used to stimulate a biological neuron that elicited muscle contraction. Despite these

[1]CAS Key Laboratory of Magnetic Materials and Devices, Ningbo Institute of Materials Technology and Engineering, Chinese Academy of Sciences, Ningbo 315201, P. R. China. [2]Zhejiang Province Key Laboratory of Magnetic Materials and Application Technology, Ningbo Institute of Materials Technology and Engineering, Chinese Academy of Sciences, Ningbo 315201, P. R. China. [3]University of Chinese Academy of Sciences, Beijing 100049, P. R. China. [4]National Institute for Materials Science, 1-1 Namiki, Tsukuba, Ibaraki 305-0044, Japan.
*Corresponding author. Email: liuyw@nimte.ac.cn (Y.L.); runweili@nimte.ac.cn (R.-W.L.)

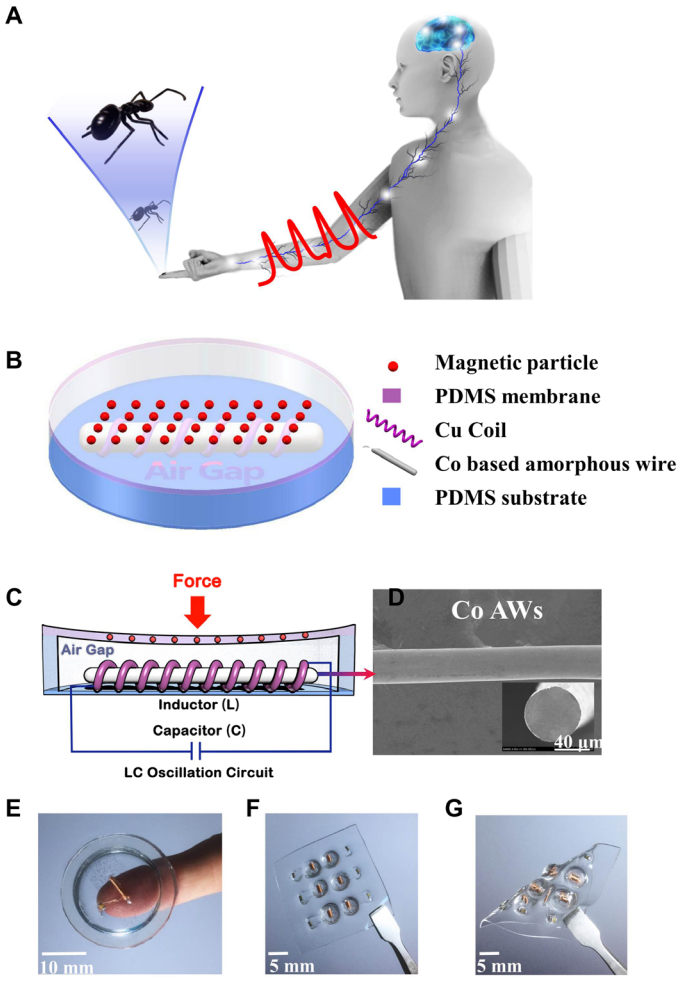

Fig. 1. Schematic illustrations and photographs of the skin-inspired tactile sensor. (**A**) Schematic illustration of a human touch sensation. (**B**) Schematic illustration of the tactile sensor. (**C**) Schematic illustration of the sensing mechanism used for tactile sensing. (**D**) Scanning electron microscope (SEM) image of the surface of Co AW. Inset: SEM image of the fractured surface. (**E**) Photograph showing the current sensor. (**F**) Photograph of the sensor array. (**G**) Photograph showing the flexibility of the sensor array.

achievements, newly developed bionic tactile-perception systems for e-skins with integrated stimuli sensing and neuron-like information-encoding stimuli functionalities in the low-pressure regime still face challenges. Challenges include limited digital-frequency transduction mechanisms and their compatible integration with the sensing capacity of high sensitivity and low detection limit.

Here, we demonstrate a tactile sensor based on magnetic sensing technology for smart prosthetics that exhibited high sensitivity and low detection limit with transduction of digital-frequency signals in the low-pressure regime. The tactile sensor based on the proposed concept demonstrated a sensitivity of 4.4 kPa^{-1} (equal to 120 N^{-1}) and a detection limit of 0.3 Pa (equivalently 10 μN) in the range of 0 to ~1 kPa. The direct transduction of force stimuli into digital-frequency signals was achieved by the integration of the tactile sensor with an LC oscillation circuit. The frequency increased with an increase in external force, and it remained consistent with the relationship between stimuli and human responses. The proposed tactile sensor not only showed high sensitivity and low detection limit but also exhibited the pulse-like stimuli responses of humans, which confirms its potential for applications in smart prosthetics, even beyond the sensing capacity of tactile mechanoreceptors (such as slow-adapting ones) in natural limbs.

RESULTS

Design and measuring principle of the skin-inspired tactile sensor

The digital tactile sensor was composed of the free-standing membrane of a polymer magnet and a magnetic sensor integrated in the air gap structure (Fig. 1B). An air gap was introduced to obtain a low detection limit because the free-standing membrane of the polymer magnet, which was embedded on top of the air gap, deformed easily under the action of an external force. The magnetic sensor, embedded with the air gap at the bottom, sensed the change of magnetic field due to deformation of the polymer magnet induced by the subtle force. The LC oscillation circuit was composed of a circuit in which an inductor (L) and a capacitor (C) were applied in parallel. This circuit has been used to convert time-domain signals into frequency-domain signals as described in Eq. 1,

$$f = \frac{1}{2\pi\sqrt{LC}} \quad (1)$$

where L is inductance and C is capacitance. The magnetic sensor was chosen to be inductive so that the inductive element sensed the change of magnetic field and formed an LC oscillation circuit with the capacitor. Giant magneto-impedance (GMI) material, which offers several advantages over conventional magnetic material, including a high sensitivity of 500%/Oe, was used as the inductive sensing element. The GMI material provided a sensitive route to detect the subtle change of magnetic field (*42*, *43*). As shown in Fig. 1C and fig. S1, the magnetic flux change from the polymer magnet passing through the inductive sensing element changed the impedance of the sensing element due to the GMI effect. When an external force was applied to the polymer magnet, the free-standing membrane deformed inward, which resulted in the displacement of the polymer magnet toward the inductive sensing element (fig. S1B). As a result, magnetic flux passing through the inductive sensing element increased, and impedance of the sensing element decreased. In this proposed device scheme, the frequency of the LC oscillation circuit also changed with the amount of external force.

Co-based amorphous wire (Co AW), a type of GMI material that exhibits high permeability and excellent GMI effect (*44*–*47*), was used as the core of the inductive sensing element. The Co AW has a uniform and smooth surface with a diameter of 60 μm (Fig. 1D) and exhibited high permeability (fig. S2). The fabrication process for the tactile sensor based on Co AW and the air gap structure is shown in fig. S3. A PDMS ring was replicated from a plastic mold and then grafted to a micrometer-thick PDMS membrane at the bottom to hold up the inductive sensing element. The polymer magnet, which consisted of PDMS and neodymium iron boron (NdFeB) magnetic powder, was placed on top of the PDMS ring and formed the free-standing membrane. The PDMS ring and the free-standing membrane together formed an air gap structure that allowed the free-standing membrane to deform easily under an external force. The resulting devices are

flexible and can have different sizes and geometries for different prosthetic applications (Fig. 1, E to G).

The magnetic gradient of polymer magnets is a key parameter for sensing capacity. The magnetic gradients of the polymer magnet with perpendicular and parallel magnetization directions were simulated by Ansoft software (fig. S4). The magnetic gradient of the perpendicular magnetization was much larger than that of the parallel magnetization. Therefore, the polymer magnet was magnetized perpendicularly to the plane of the membrane by a magnetic field of 2 T. The magnetization loop, the remanence, and the retentivity of the polymer magnet were also studied (fig. S5).

Characterization and optimization of the device

The magnetic field sensitivity of the inductive sensing element was investigated. A sinusoidal driving current of 1 mA with frequency ranging from 0.5 kHz to 5 MHz was passed through the inductive sensing element, and the impedance was measured at different magnetic fields ranging from 40 to −40 Oe. The percentage change of magneto-impedance (i.e., GMI ratio) is defined as

$$\frac{\Delta Z}{Z}(\%) = \frac{Z(H_{ex}) - Z(H_{sat})}{Z(H_{sat})} \times 100\% \qquad (2)$$

where $Z(H_{ex})$ and $Z(H_{sat})$ are the impedance values under an external magnetic field H_{ex} and the saturated magnetic field H_{sat}, respectively. The GMI ratio decreased almost linearly with an increase in magnetic field from 0 to 6.2 Oe, and, when the magnetic field was larger than 6.2 Oe, the GMI ratio remained zero, indicating saturation of the core (fig. S6). As shown in Fig. 2A, the GMI ratio increased with the frequency until the frequency reached 250 kHz; the GMI ratio reached as high as 500% and saturated under the magnetic field of 6.2 Oe, as a consequence of the contribution of the permeability of Co AW based on the skin effect (*38*). Then, the GMI ratio decreased with an increase in exciting frequency. The GMI ratio also increased with the driving current. Until the driving current reached 1 mA, the GMI ratio reached 500% at 250 kHz. When the driving current increased further, the GMI ratio decreased (fig. S7).

The magnetic field sensitivity of the inductive sensing element can be expressed as

$$\eta = \frac{dZ(H)}{Z(H_{sat})} \times \frac{1}{dH} \qquad (3)$$

where $Z(H_{sat})$ is the impedance of the inductive sensing element at saturation magnetic field, $dZ(H)$ is the change of impedance under an external magnetic field, and dH is the change of magnetic field. At a driving current of 1 mA and a frequency of 250 kHz, a sensitivity of 80%/Oe was obtained. The field sensitivity of the current inductive sensing element was higher compared with a giant magnetoresistance sensor that has a sensitivity of ~1%/Oe (*34*). Therefore, a subtle force can be detected by the tactile sensor with high magnetic field sensitivity and a near-linear response to magnetic field.

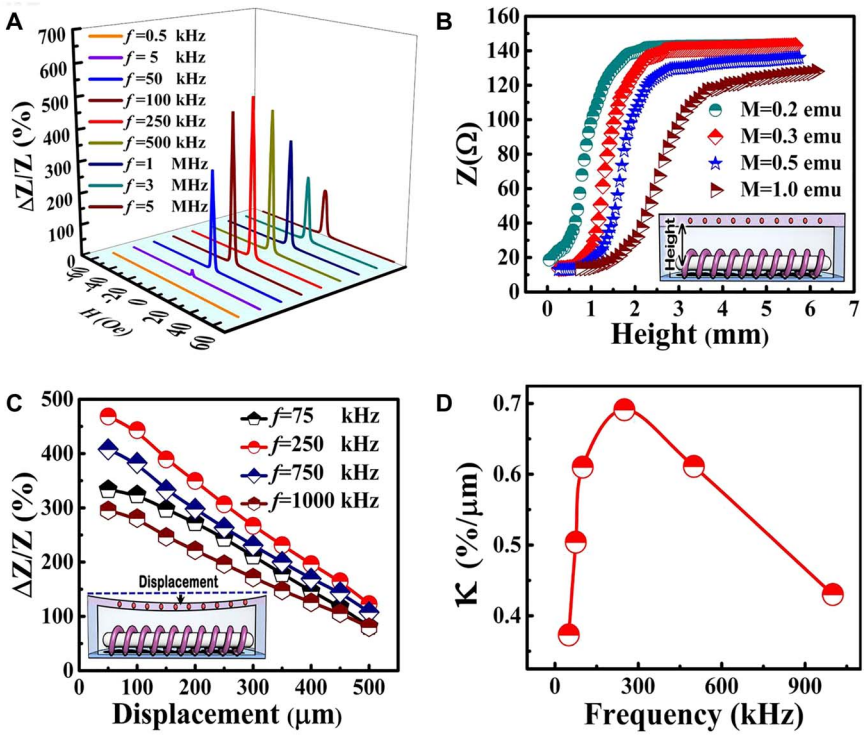

Fig. 2. Characterization and optimization of the device. (**A**) GMI ratio responses of the inductive sensing element to the magnetic field at different exciting frequencies. (**B**) Experimental impedance responses of the inductive sensing element to height changes. *M* is the remanent magnetization of the polymer magnet. Height is between the polymer magnet and the inductive sensing element. (**C**) The GMI ratio responses of the sensor to the displacements at different frequencies, that is, 75, 250, 750, and 1000 kHz. Displacement is the deformation of the polymer magnet under different loadings. (**D**) Relation of the factor of sensitivity κ of the inductive sensing element and frequency of driving current.

The parameters of the air gap are also important for the sensitivity and the detection limit of the sensor. The most important parameter is the height of the PDMS ring, defined as the distance between the polymer magnet and the inductive sensing element. The height should be optimized to ensure that the inductive sensing element works best at a biased magnetic field in the range of 0 to ~6.2 Oe. Impedance values were measured in situ when the polymer magnets with different magnetization approached the inductive sensing element. As shown in Fig. 2B, when the polymer magnet was far away from the inductive sensing element, the impedance was high. The curve shifted to the larger distance range when increasing the magnetization of the polymer magnet. Therefore, a higher PDMS ring was required for the same sensitivity when the polymer magnet had a larger magnetization. When the polymer magnet approached the sensing element, impedance initially showed almost no change. However, when the height was smaller than a critical value, the impedance showed a sublinear dependence on the height. When the height decreased to another critical value, the impedance started to show weak height dependence, which meant that the magnetic field generated by the polymer magnet reached about 6.2 Oe.

The first differential relation between impedance and height is shown in fig. S8 to understand the sensitive height range for the sensing element. When the polymer magnet was away from the sensing element (point b in fig. S8), the first differential value reached zero. In this

case, there was nearly no change in impedance. However, when the polymer magnet approached the sensing element, the differential value showed a sharp increase with the decreased distance until it reached a peak value (point c in fig. S8). After the peak value, the differential value decreased with the decrease in height until the height reached another critical value (point a in fig. S8). This means that the height of the PDMS ring should be chosen at the peak value of point c with the highest sensitivity. The polymer magnet with a magnetization of 0.3 electromagnetic unit (emu) and the PDMS ring with a height of about 1.3 mm were chosen so that the tactile sensor would work at the most sensitive range. Thus, a subtle force applied to the polymer magnet caused displacement, and impedance was changed due to the variation in magnetic field. The response of the GMI ratio to the displacement under different loadings with different frequencies is illustrated in Fig. 2C. Displacement is the distance traveled by the polymer magnet under external loading. Frequency has a significant effect on the GMI ratio response under the loading. To realize the effect of exciting frequency, the factor of sensitivity κ is defined as follows

$$\kappa = \frac{\left(\Delta Z/Z\right)_{max} - \left(\Delta Z/Z\right)_{min}}{\Delta d} \quad (4)$$

where $(\Delta Z/Z)_{max}$ and $(\Delta Z/Z)_{min}$ are the GMI ratios at the maximum and minimum displacements, respectively, and Δd is the difference between minimum and maximum displacement. Values of κ increased from 0.37 to 0.69%/μm with the frequency ranging from 50 to 250 kHz and then decreased when the frequency was higher than 250 kHz (Fig. 2D). Therefore, the optimal frequency is 250 kHz, consistent with the optimal frequency of the inductive sensing element.

Ultralow pressure sensing ability

First, the sensitivity of the tactile sensor was investigated. The vertical forces were loaded on the sensor by a microstress sensor measurement system. The impedance was measured in situ with the application of loading on the tactile sensor. The distance between the sensing element and the polymer magnet decreased slightly in the presence of loading, and the magnetic flux passing through the sensing element increased, which lastly induced the change in impedance. The impedance change (ΔZ%) of the sensor was defined as

$$\Delta Z(\%) = \left|\frac{Z - Z_0}{Z_0}\right| \times 100\% \quad (5)$$

where Z and Z_0 are impedance values with and without the application of external force, respectively. The impedance change increased with an increase in subtle pressure (Fig. 3A). An approximately linear relationship between ΔZ% and applied pressure P in the range of 0 to ~7.5 Pa was observed. The sensor showed noise of almost 0.02% without loading, but when a pressure of 0.3 Pa was applied, the sensor showed 0.15% relative change in impedance (fig. S9). This demonstrates that the sensor was able to distinguish between subtle pressure and noise. The sensitivity of the tactile sensor is defined as $S = \Delta(\Delta Z\%)/\Delta P$, where Δ (ΔZ%) is the relative impedance change and ΔP is the change in applied pressure. The sensitivity is 4.4 kPa^{-1}, equal to 120 N^{-1} (the contact area is about 4×10^{-5} m^2). The prosthetics not only perceived ultralow pressure but also had the ability to grasp heavy objects. Therefore, the sensor is also prepared to detect pressure

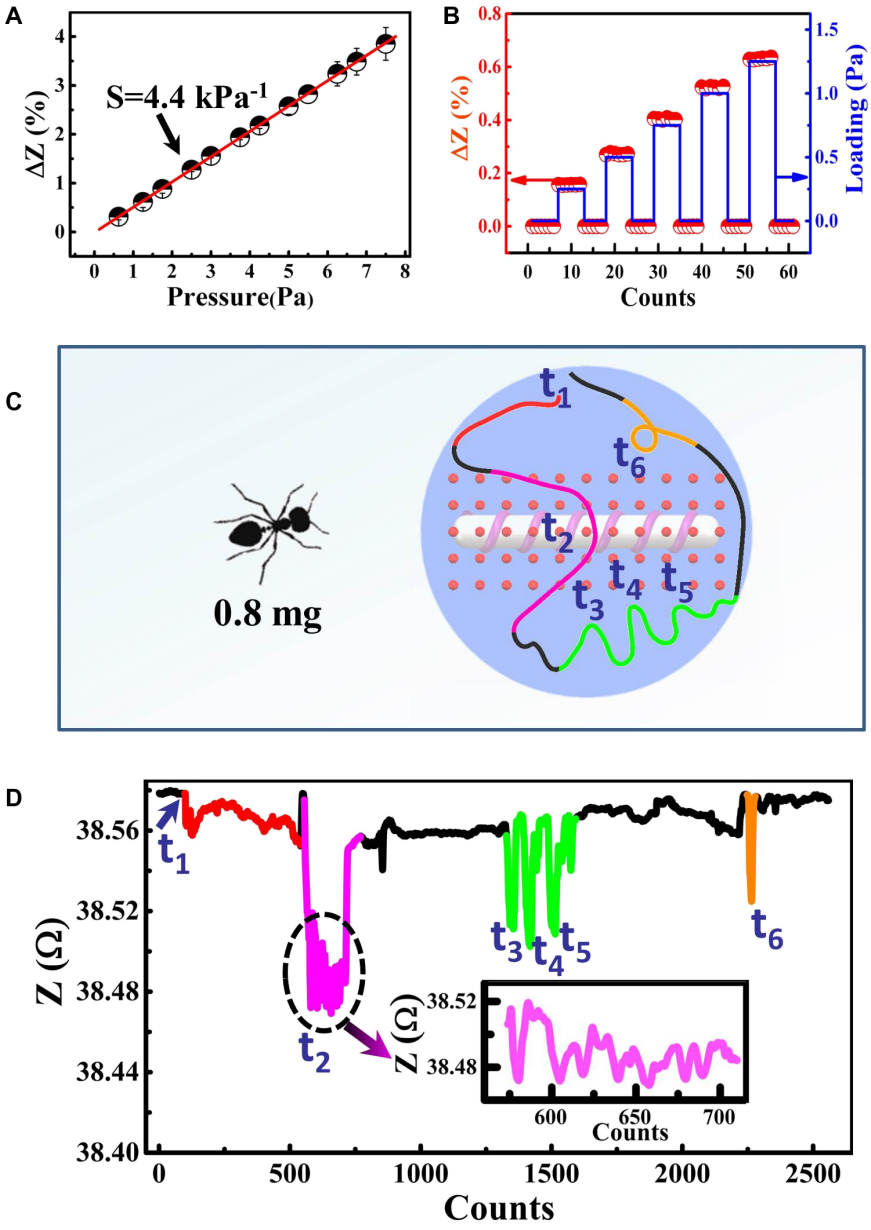

Fig. 3. Evaluation of sensing performance. (**A**) Relation between changes in impedance and applied pressures shows the sensitivity of the tactile sensor in the ultralow pressure range. (**B**) Response of the pressure sensor to water droplets, each with a volume of 1 μl. The corresponding pressure is calculated to be equal to 0.3 Pa. (**C**) Schematic illustration of the trail of a moving ant. (**D**) The responses of the tactile sensor to the moving ant.

over 20 kPa (fig. S10). The durability and the stability of the sensor are also important for practical applications. The reported sensor exhibited (fig. S11) high durability and stability under a loading of 25 Pa by repeated load cycling 10^5 times. Besides this, the sensor was mounted on a mechanical arm to demonstrate the wearable pressure sensing performance. When the finger was touched gently, the sensor signaled a response (fig. S12B). The sensor could also perceive the wind blowing, as shown in fig. S12C.

The detection limit of the tactile sensor was further investigated by dropping water of different volumes (1 μl, equal to 10 μN) onto the tactile sensor. The impedance was measured after several seconds, when the water droplet was uniformly distributed. A change of 0.15% in the impedance was obtained for a volume of 1 μl (fig. 3B). The impedance change increased with increasing volumes of water droplets. The tactile sensor could distinguish a weight of 10 μN. By taking the contact area as about equal to 4×10^{-5} m^2, we calculated the corresponding pressure detection limit to be equal to 0.3 Pa.

The dynamic sensing was demonstrated by placing small live insects of 0.8-mg mass onto the tactile sensor. The actions of the ant could be sensed. Figure 3C shows the moving trail of the ant, and Fig. 3D demonstrates the change of impedance of the tactile sensor with the moving ant. The impedance of the tactile sensor is about 38.57 ohms. When the ant was placed at the edge of the sensor (t_1), an impedance change of 0.02 ohms was recorded. Then, the ant moved around the edge of the sensor. When the ant stayed at the center of the sensor (t_2), a large deformation occured and the impedance of the sensor dropped markedly to 38.48 ohms. When the ant stayed at the center of the polymer magnet for several seconds, the impedance of the tactile sensor continued to fluctuate slightly with the ant antenna touching the free-standing membrane of polymer magnet (Fig. 3D, inset). The backward and forward movement of the ant near the center of the ring (three times) led to dynamic changes in impedance, as confirmed by the three peaks (t_3, t_4, and t_5) in Fig. 3D. The impedance change was larger when the ant was closer to the center of the ring and when the ant was placed upside down on the membrane. The ant struggled, strongly scratching the membrane, moving, and trying to turn over (t_6). Last, the ant turned over and moved freely. After this, the impedance dropped slowly.

The bionic behavior of the skin-inspired tactile sensor

Tee *et al.* (*40*) reported that the action potential of neurons was closely followed by the frequency of pulses. In this way, the study provided a technique to encode pressure into digital-frequency pulse signals and to add sensing capabilities to prosthetic devices. In this work, analog signals recorded from the sensor were converted into digital-frequency signals by using an LC oscillation circuit composed of a tactile sensor and a capacitor of 100 nF. A tactile sensor served as the inductor (L) in the circuit. The LC circuit frequency was modulated according to the change of inductance. As shown in Fig. 4A, the high-frequency sinusoidal signal from the LC oscillation circuit was converted into a square signal with high frequency. The square signal was consequently divided into a low-frequency signal by the frequency division circuit, which was then converted into pulse waveforms. The pulse waveforms changing with pressure were considered the output. Fig. 4B demonstrates the frequency changes under loadings of 50, 113, and 1000 Pa. The number of pulse waveforms increased with loading, which is similar to human responses to force stimuli. The relationship between loading and frequency was further investigated (Fig. 4C). The frequency of pulse waveforms increased with loading in the range of 0 to ~1 kPa. The exponential function of $f = 69 - 20\,e^{-(P-62)/424}$ was obtained, where f is the frequency response (in hertz) and P is pressure stimuli (in pascals), consistent with the stimuli-response function in the literature (*48*). A pressure of more

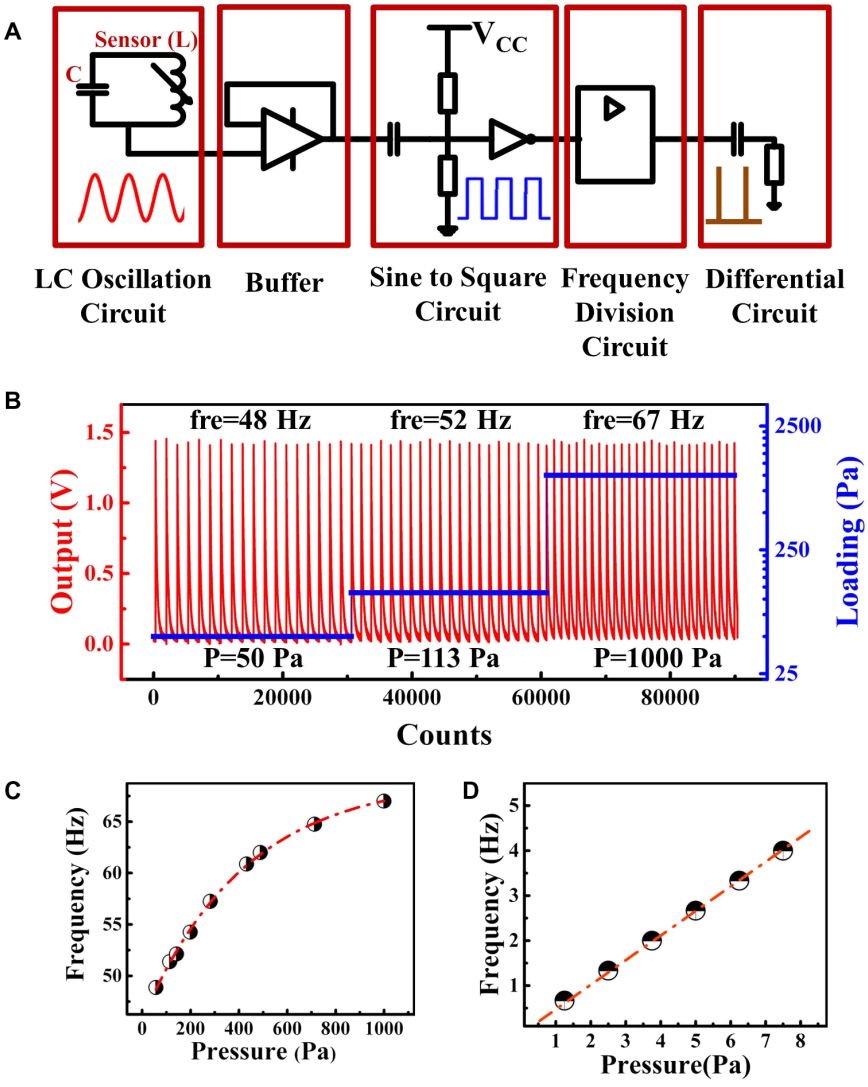

Fig. 4. The biomimetic pressure sensing ability. (**A**) Schematic diagram showing the circuit that converts analog signals recorded from the sensor into digital-frequency signals. (**B**) The digital-frequency response of the device changed with applied pressure, a pressure range experienced by humans in their daily lives. (**C**) The digital frequency as a function of applied pressure in the range of 0 to ~1 kPa. (**D**) The digital frequency as a function of applied pressure in the range of 0 to ~7.5 Pa.

than 20 kPa was also transformed into a digital-frequency signal for practical applications in which a heavy object was grasped, as shown in fig. S13.

When a subtle pressure was placed on the sensor, a digital pulse waveform similar to a human's was obtained by another used logic circuit shown in fig. S14. When the number of pulse waveforms from the first counter was more than the base number of pulse waveforms without loading, the second counter was triggered and it started to count pulse waveforms. The change in the number of pulse waveforms under the subtle pressure was investigated through the logic circuit. Frequency changed with an increase in subtle pressure, ranging from 0 to ~7.5 Pa (Fig. 4D). When a loading of 1.25 Pa was placed on the tactile sensor, a 0.7-Hz pulse waveform was obtained by the device. Therefore, a minimum loading of 1.25 Pa (the contact area is about 4×10^{-5} m^2 or 50 μN), beyond the sensing threshold value of humans (1 mN) (*1*), can be encoded as digital-frequency signals.

DISCUSSION

Recent neuroprosthetic studies showed that pressure sensation can be stimulated by injecting a train of pulses having different frequencies via cuff interfaces (*49*) and that pain sensation can be elicited through transcutaneous electrical nerve stimulation (*39*). In addition, reconstruction of tactile sensation of force levels and object shape was shown by using multielectrode stimulation via pulses in which current amplitude increased linearly with sensor outputs (*35*). In contrast, this work focused on providing a biomimetic tactile sensory system to sense subtle pressure stimuli via digital pulses for functional prosthetics. Subtle pressure sensing is a remarkable skill of our somatosensory system, which is used in everyday activities to interact with the environment. The reported tactile sensor exhibited a very high sensitivity of 4.4 kPa^{-1} and an ultralow detection limit of 0.3 Pa. Factors that played an important role in enhancement of tactile sensor performance are as follows: (i) Co AW with an excellent GMI effect, that is, the inductive sensing element with high sensitivity to magnetic field sensed the weak magnetic field, ensuring the high sensitivity of the sensor; (ii) the free-standing membrane of the air gap deformed easily under an external subtle force due to a slight loss of the subtle force, providing the low detection limit of the sensor; and (iii) the inductive sensing element sensed the magnetic field change induced by the subtle force and simultaneously changed the frequency of the LC oscillation circuit. Compatibility of sensing pressure stimuli and simultaneous transduction of digital-frequency signals makes the current sensor innovative and applicable for smart prosthetics.

Furthermore, the digital pulse signals from artificial tactile sensors, which are compatible with humans, were obtained by an LC oscillation circuit. The frequency increased with the external force, consistent with the relationship between stimuli and human responses. Previously, some researchers used a microneurographic method to obtain the pressure response of slowly and rapidly adapting cutaneous mechanoreceptors in the human body (*50*, *51*). They have shown that the receptors increased their discharge frequency when pressure was applied to their receptive field. Our results are consistent with those of previous studies. The free-standing membrane of the polymer magnet was similar to the receptive field: When pressure was applied, the frequency of the pulse signals of the device increased.

Overall, the performance of the reported tactile sensor indicates potential applications in the field of smart prosthetics. Besides, we expect that the sensitivity and detection limit of the sensor can be further improved by choosing GMI materials with a higher GMI ratio and by varying the thickness of the PDMS membrane through optimization of the polymer magnet and the fabrication method. Sensory feedback of tactile sensors with high sensitivity, low detection limit, and digital-frequency signals may make prosthetic limbs better and more personalized in the future.

MATERIALS AND METHODS

Preparation of the PDMS ring

The PDMS pre-polymer and its curing agent (Sylgard 184, Dow Corning) were poured in the plastic mold in a ratio of 8:1 (w/w). Poured PDMS were cured in a vacuum oven at 80°C for 12 hours. Last, the mold was shaken in methanol, and the ring was carefully removed.

Preparation of free-standing membrane

Fabrication of the PDMS membrane (~20 μm) was carried out according to the steps reported in the literature (*52*, *53*): (i) A 1-μm-thick sacrificial layer of SU-8 photoresist was spin-coated onto a clear silicon wafer. (ii) PDMS solution was diluted with hexane before spin-coating. A PDMS pre-polymer–to–curing agent ratio of 10:1 (w/w) was used. PDMS/hexane solution (2:1, w/w) (800 μl) was spin-coated onto a sacrificial layer at 2000 revolutions per minute for 3 min and then cured at 80°C for 12 hours. (iii) The membrane was shaken in acetone and methanol and then carefully removed.

Preparation of the polymer magnet

PDMS was prepared by mixing the base and curing agent at a 10:1 weight ratio. NdFeB powder and PDMS were mixed at different weight ratios. Then, the mixture was fabricated by using a master mold technique. After 2 hours of curing at 80°C, the polymer magnet was magnetized by applying a magnetic field of 2 T. The polymer magnet was bonded onto the free-standing membrane by using an intermediate pre-polymerized PDMS and cured for 2 hours.

Preparation of the inductive sensing element

A 100-μm copper wire was wound around 500-μm microtubes in the same direction by using a winding machine, forming a tight coil with a length of 10 mm. The number of turns could be controlled by the winding machine, ensuring repeatability and consistency of the coil. Co AW with a diameter of 60 μm was prepared by the melt extraction method. Then, Co AW was cut to size for the core of the inductive coil, forming the inductive sensing element. The polymer magnet was placed on top, and the inductive sensing element was placed at the bottom of the PDMS ring. The LC oscillation circuit comprised a circuit in which an inductive sensing element (L) and a capacitor (C) were at the bottom of the PDMS ring with a parallel combination.

Device characterization

Impedance measurement was conducted with a Hioki IM3570 impedance analyzer. Loading was manually measured. The device was powered by a 5-V battery in the experiment. We designed a readout circuit based on transistors and a liquid crystal display to display the output of the device.

SUPPLEMENTARY MATERIALS

robotics.sciencemag.org/cgi/content/full/3/22/eaat0429/DC1

Additional methods

Fig. S1. Schematic illustration of the operating mechanism of the device.

Fig. S2. Characterization of Co AW.
Fig. S3. Schematic illustration of the fabrication procedure of the tactile sensor.
Fig. S4. Comparison of the magnetic gradient of the polymer magnet with the perpendicular and parallel magnetization.
Fig. S5. Characterization of the polymer magnet.
Fig. S6. GMI ratio of the inductive sensing element at different magnetic field values.
Fig. S7. The GMI ratio of the inductive sensing element at different driving current values.
Fig. S8. The first differential relations between the impedance of the inductive sensing element and the height obtained as a result of calculation from Fig. 2B.
Fig. S9. The real-time response of the sensor to the subtle pressure.
Fig. S10. The response of the sensor to the pressure in the range of 0 to 100 kPa.
Fig. S11. The durability and stability of the current sensor.
Fig. S12. The wearable pressure sensing performance of sensors.
Fig. S13. The digital frequency as a function of applied pressure in the range of 10 to 180 kPa.
Fig. S14. The logic circuit for the pulse waveform of the subtle pressure.

REFERENCES AND NOTES

1. A. Chortos, J. Liu, Z. Bao, Pursuing prosthetic electronic skin. *Nat. Mater.* **15**, 937–950 (2016).
2. A. P. Gerratt, H. O. Michaud, S. P. Lacour, Elastomeric electronic skin for prosthetic tactile sensation. *Adv. Funct. Mater.* **25**, 2287–2295 (2015).
3. G. Zhu, W. Q. Yang, T. Zhang, Q. Jing, J. Chen, Y. S. Zhou, P. Bai, Z. L. Wang, Self-powered, ultrasensitive, flexible tactile sensors based on contact electrification. *Nano Lett.* **14**, 3208–3213 (2014).
4. B. Zhu, Z. Niu, H. Wang, W. R. Leow, H. Wang, Y. Li, L. Zheng, J. Wei, F. Huo, X. Chen, Microstructured graphene arrays for highly sensitive flexible tactile sensors. *Small* **10**, 3625–3631 (2014).
5. J. L. Collinger, M. A. Kryger, R. Barbara, T. Betler, K. Bowsher, E. H. P. Brown, S. T. Clanton, A. D. Degenhart, S. T. Foldes, R. A. Gaunt, F. E. Gyulai, E. A. Harchick, D. Harrington, J. B. Helder, T. Hemmes, M. S. Johannes, K. D. Katyal, G. S. F. Ling, A. J. C. McMorland, K. Palko, M. P. Para, J. Scheuermann, A. B. Schwartz, E. R. Skidmore, F. Solzbacher, A. V. Srikameswaran, D. P. Swanson, S. Swetz, E. C. Tyler-Kabara, M. Velliste, W. Wang, D. J. Weber, B. Wodlinger, M. L. Boninger, Collaborative approach in the development of high-performance brain-computer interfaces for a neuroprosthetic arm: Translation from animal models to human control. *Clin. Transl. Sci.* **7**, 52–59 (2014).
6. M. Velliste, S. Perel, M. C. Spalding, A. S. Whitford, A. B. Schwartz, Cortical control of a prosthetic arm for self-feeding. *Nature* **453**, 1098–1101 (2008).
7. X. Xiao, L. Yuan, J. Zhong, T. Ding, Y. Liu, Z. Cai, Y. Rong, H. Han, J. Zhou, Z. L. Wang, High-strain sensors based on ZnO nanowire/polystyrene hybridized flexible films. *Adv. Mater.* **23**, 5440–5444 (2011).
8. B. C.-K. Tee, C. Wang, R. Allen, Z. Bao, An electrically and mechanically self-healing composite with pressure- and flexion-sensitive properties for electronic skin applications. *Nat. Nanotechnol.* **7**, 825–832 (2012).
9. M. Amjadi, A. Pichitpajongkit, S. Lee, S. Ryu, I. Park, Highly stretchable and sensitive strain sensor based on silver nanowire-elastomer nanocomposite. *ACS Nano* **8**, 5154–5163 (2014).
10. Y. Zang, F. Zhang, C.-a. Di, D. Zhu, Advances of flexible pressure sensors toward artificial intelligence and health care applications. *Mater. Horiz.* **2**, 140–156 (2015).
11. J. Kim, M. Lee, H. J. Shim, R. Ghaffari, H. R. Cho, D. Son, Y. H. Jung, M. Soh, C. Choi, S. Jung, K. Chu, D. Jeon, S.-T. Lee, J. H. Kim, S. H. Choi, T. Hyeon, D.-H. Kim, Stretchable silicon nanoribbon electronics for skin prosthesis. *Nat. Commun.* **5**, 5747 (2014).
12. M. A. McEvoy, N. Correll, Materials that couple sensing, actuation, computation, and communication. *Science* **347**, 1261689 (2015).
13. C. Pang, G.-Y. Lee, T.-i. Kim, S. M. Kim, H. N. Kim, S.-H. Ahn, K.-Y. Suh, A flexible and highly sensitive strain-gauge sensor using reversible interlocking of nanofibres. *Nat. Mater.* **11**, 795–801 (2012).
14. X. Liao, Q. Liao, X. Yan, Q. Liang, H. Si, M. Li, H. Wu, S. Cao, Y. Zhang, Flexible and highly sensitive strain sensors fabricated by pencil drawn for wearable monitor. *Adv. Funct. Mater.* **25**, 2395–2401 (2015).
15. C. Pang, J. H. Koo, A. Nguyen, J. M. Caves, M.-G. Kim, A. Chortos, K. Kim, P. J. Wang, J. B.-H. Tok, Z. Bao, Highly skin-conformal microhairy sensor for pulse signal amplification. *Adv. Mater.* **27**, 634–640 (2015).
16. C. M. Boutry, A. Nguyen, Q. O. Lawal, A. Chortos, S. Rondeau-Gagné, Z. Bao, A sensitive and biodegradable pressure sensor array for cardiovascular monitoring. *Adv. Mater.* **27**, 6954–6961 (2015).
17. Y. Zang, F. Zhang, D. Huang, X. Gao, C.-a. Di, D. Zhu, Flexible suspended gate organic thin-film transistors for ultra-sensitive pressure detection. *Nat. Commun.* **6**, 6269 (2015).
18. T. Someya, T. Sekitani, S. Iba, Y. Kato, H. Kawaguchi, T. Sakurai, A large-area, flexible pressure sensor matrix with organic field-effect transistors for artificial skin applications. *Proc. Natl. Acad. Sci. U.S.A.* **101**, 9966–9970 (2004).
19. S. Ryu, P. Lee, J. B. Chou, R. Xu, R. Zhao, A. J. Hart, S.-G. Kim, Extremely elastic wearable carbon nanotube fiber strain sensor for monitoring of human motion. *ACS Nano* **9**, 5929–5936 (2015).
20. S. Lee, A. Reuveny, J. Reeder, S. Lee, H. Jin, Q. Liu, T. Yokota, T. Sekitani, T. Isoyama, Y. Abe, Z. Suo, T. Someya, A transparent bending-insensitive pressure sensor. *Nat. Nanotechnol.* **11**, 472–478 (2016).
21. H. Jang, Y. J. Park, X. Chen, T. Das, M.-S. Kim, J.-H. Ahn, Graphene-based flexible and stretchable electronics. *Adv. Mater.* **28**, 4184–4202 (2016).
22. N. Lu, C. Lu, S. Yang, J. Rogers, Highly sensitive skin-mountable strain gauges based entirely on elastomers. *Adv. Funct. Mater.* **22**, 4044–4050 (2012).
23. S. Yao, Y. Zhu, Wearable multifunctional sensors using printed stretchable conductors made of silver nanowires. *Nanoscale* **6**, 2345–2352 (2014).
24. Z. Zou, C. Zhu, Y. Li, X. Lei, W. Zhang, J. Xiao, Rehealable, fully recyclable, and malleable electronic skin enabled by dynamic covalent thermoset nanocomposite. *Sci. Adv.* **4**, eaaq0508 (2018).
25. L. Pan, A. Chortos, G. Yu, Y. Wang, S. Isaacson, R. Allen, Y. Shi, R. Dauskardt, Z. Bao, An ultra-sensitive resistive pressure sensor based on hollow-sphere microstructure induced elasticity in conducting polymer film. *Nat. Commun.* **5**, 3002 (2014).
26. X. Wang, L. Dong, H. Zhang, R. Yu, C. Pan, Z. L. Wang, Recent progress in electronic skin. *Adv. Sci.* **2**, 1500169 (2015).
27. Z. Zhu, R. Li, T. Pan, Imperceptible epidermal–iontronic interface for wearable sensing. *Adv. Mater.* **30**, 1705122 (2018).
28. L. Persano, C. Dagdeviren, Y. Su, Y. Zhang, S. Girardo, D. Pisignano, Y. Huang, J. A. Rogers, High performance piezoelectric devices based on aligned arrays of nanofibers of poly(vinylidenefluoride-co-trifluoroethylene). *Nat. Commun.* **4**, 1633 (2013).
29. S. C. B. Mannsfeld, B. C.-K. Tee, R. M. Stoltenberg, C. V. H.-H. Chen, S. Barman, B. V. O. Muir, A. N. Sokolov, C. Reese, Z. Bao, Highly sensitive flexible pressure sensors with microstructured rubber dielectric layers. *Nat. Mater.* **9**, 859–864 (2010).
30. G. Schwartz, B. C.-K. Tee, J. Mei, A. L. Appleton, D. H. Kim, H. Wang, Z. Bao, Flexible polymer transistors with high pressure sensitivity for application in electronic skin and health monitoring. *Nat. Commun.* **4**, 1859 (2013).
31. S. Park, H. Kim, M. Vosgueritchian, S. Cheon, H. Kim, J. H. Koo, T. R. Kim, S. Lee, G. Schwartz, H. Chang, Z. Bao, Stretchable energy-harvesting tactile electronic skin capable of differentiating multiple mechanical stimuli modes. *Adv. Mater.* **26**, 7324–7332 (2014).
32. X. Wang, Y. Gu, Z. Xiong, Z. Cui, T. Zhang, Silk-molded flexible, ultrasensitive, and highly stable electronic skin for monitoring human physiological signals. *Adv. Mater.* **26**, 1336–1342 (2014).
33. A. Miyamoto, S. Lee, N. F. Cooray, S. Lee, M. Mori, N. Matsuhisa, H. Jin, L. Yoda, T. Yokota, A. Itoh, M. Sekino, H. Kawasaki, T. Ebihara, M. Amagai, T. Someya, Inflammation-free, gas-permeable, lightweight, stretchable on-skin electronics with nanomeshes. *Nat. Nanotechnol.* **12**, 907–913 (2017).
34. R. Saraf, L. Pu, V. Maheshwari, A light harvesting, self-powered monolith tactile sensor based on electric field induced effects in $MAPbI_3$ perovskite. *Adv. Mater.* **30**, 1705778 (2018).
35. S. Raspopovic, M. Capogrosso, F. M. Petrini, M. Bonizzato, J. Rigosa, G. Di Pino, J. Carpaneto, M. Controzzi, T. Boretius, E. Fernandez, G. Granata, C. M. Oddo, L. Citi, A. L. Ciancio, C. Cipriani, M. C. Carrozza, W. Jensen, E. Guglielmelli, T. Stieglitz, P. M. Rossini, S. Micera, Restoring natural sensory feedback in real-time bidirectional hand prostheses. *Sci. Transl. Med.* **6**, 222ra19 (2014).
36. S. N. Flesher, J. L. Collinger, S. T. Foldes, J. M. Weiss, J. E. Downey, E. C. Tyler-Kabara, S. J. Bensmaia, A. B. Schwartz, M. L. Boninger, R. A. Gaunt, Intracortical microstimulation of human somatosensory cortex. *Sci. Transl. Med.* **8**, 361ra141 (2016).
37. G. S. Dhillon, K. W. Horch, Direct neural sensory feedback and control of a prosthetic arm. *IEEE Trans. Neural Syst. Rehab. Eng.* **13**, 468–472 (2005).
38. C. M. Oddo, S. Raspopovic, F. Artoni, A. Mazzoni, G. Spigler, F. Petrini, F. Giambattistelli, F. Vecchio, F. Miraglia, L. Zollo, G. Di Pino, D. Camboni, M. C. Carrozza, E. Guglielmelli, P. M. Rossini, U. Faraguna, S. Micera, Intraneural stimulation elicits discrimination of textural features by artificial fingertip in intact and amputee humans. *eLife* **5**, e09148 (2016).
39. L. E. Osborn, A. Dragomir, J. L. Betthauser, C. L. Hunt, H. H. Nguyen, R. R. Kaliki, N. V. Thakor, Prosthesis with neuromorphic multilayered e-dermis perceives touch and pain. *Sci. Robot.* **3**, eaat3818 (2018).
40. B. C.-K. Tee, A. Chortos, A. Berndt, A. K. Nguyen, A. Tom, A. McGuire, Z. C. Lin, K. Tien, W.-G. Bae, H. Wang, P. Mei, H.-H. Chou, B. Cui, K. Deisseroth, T. N. Ng, Z. Bao, A skin-inspired organic digital mechanoreceptor. *Science* **350**, 313–316 (2015).
41. Y. Kim, A. Chortos, W. Xu, Y. Liu, J. Y. Oh, D. Son, J. Kang, A. M. Foudeh, C. Zhu, Y. Lee, S. Niu, J. Liu, R. Pfattner, Z. Bao, T.-W. Lee, A bioinspired flexible organic artificial afferent nerve. *Science* **360**, 998–1003 (2018).
42. M.-H. Phan, H.-X. Peng, Giant magnetoimpedance materials: Fundamentals and applications. *Prog. Mater. Sci.* **53**, 323–420 (2008).
43. S. M. Hoque, A. K. M. R. Haque, M. O. Rahman, N. H. Nghi, M. A. Hakim, S. Akhter, Ultra-soft magnetic properties and giant magneto-impedance of $Co_{68}Fe_{4.5}Si_{12.5}B_{15}$. *J. Non-Cryst. Solids* **357**, 2109–2114 (2011).

44. J. S. Liu, F. Y. Cao, D. W. Xing, L. Y. Zhang, F. X. Qin, H. X. Peng, X. Xue, J. F. Sun, Enhancing GMI properties of melt-extracted Co-based amorphous wires by twin-zone Joule annealing. *J. Alloy. Compd.* **541**, 215–221 (2012).
45. Q. Man, H. Sun, Y. Dong, B. Shen, H. Kimura, A. Makino, A. Inoue, Enhancement of glass-forming ability of CoFeBSiNb bulk glassy alloys with excellent soft-magnetic properties and superhigh strength. *Intermetallics* **18**, 1876–1879 (2010).
46. H. Wang, F. Qin, D. W. Xing, F. Y. Cao, X. D. Wang, H.-X. Peng, J. F. Sun, Relating residual stress and microstructure to mechanical and giant magneto-impedance properties in cold-drawn Co-based amorphous microwires. *Acta Mater.* **60**, 5425–5436 (2012).
47. Y. Zhao, H. Hao, Y. Zhang, Preparation and giant magneto-impedance behavior of Co-based amorphous wires. *Intermetallics* **42**, 62–67 (2013).
48. M. Knibestöl, Stimulus-response functions of slowly adapting mechanoreceptors in human glabrous skin area. *J. Physiol.* **245**, 63–80 (1975).
49. D. W. Tan, M. A. Schiefer, M. W. Keith, J. R. Anderson, J. Tyler, D. J. Tyler, A neural interface provides long-term stable natural touch perception. *Sci. Transl. Med.* **6**, 257ra138 (2014).
50. M. J. Rowe, D. J. Tracey, D. A. Mahns, V. Sahai, J. J. Ivanusic, Mechanosensory perception: Are there contributions from bone-associated receptors? *Clin. Exp. Pharmacol. Physiol.* **32**, 100–108 (2005).
51. J. P. Vedel, J. P. Roll, Response to pressure and vibration of slowly adapting cutaneous mechanoreceptors in the human foot. *Neurosci. Lett.* **34**, 289–294 (1982).
52. E. Kang, J. Ryoo, G. S. Jeong, Y. Y. Choi, S. M. Jeong, J. Ju, S. Chung, S. Takayama, S.-H. Lee, Large-scale, ultrapliable, and free-standing nanomembranes. *Adv. Mater.* **25**, 2167–2173 (2013).
53. J. Y. Park, D. H. Lee, E. J. Lee, S.-H. Lee, Study of cellular behaviors on concave and convex microstructures fabricated from elastic PDMS membranes. *Lab Chip* **9**, 2043–2049 (2009).

Acknowledgments: We acknowledge the advice and assistance of A. He in the analysis of the magnetic gradient of the polymer magnet. We also thank Z. Tang (senior engineer, Medical School of Ningbo University) for assistance with the electrophysiological experiment. **Funding:** This research was partially supported by the National Natural Foundation of China (61704177, 51525103, 11474295, and 61774161), the China International Cooperation Project (2016YFE0126700), the National Key Technologies R&D Program of China (2016YFA0201102), the Public Welfare Technical Applied Research Project of Zhejiang Province (2017C31100), Ningbo Major Science and Technology Projects (2017B10018), the Ningbo Science and Technology Innovation Team (2015B11001), and the Natural Science Foundation of Ningbo (2017A610097 and 2017A610093). **Author contributions:** Y.W., Y.L., and R.-W.L. conceived experiments and device designs. Y.W. and Y.L. carried out experiments. Y.Z. and Z.Y. performed sensitivity analysis of the inductive sensing element. Q.M. prepared Co AW, and C.H. carried out circuit signal processing. W.A., F.L., Z.Y., J.S., G.L., and M.L. provided further data analysis. Y.W., Y.L., M.L., and R.-W.L. wrote the manuscript with input from all the other authors. All authors contributed to, and agree with, the content of the final version of the manuscript. **Competing interests:** The authors declare that they have no competing financial interests. **Data and materials availability:** All data needed to evaluate the conclusions presented are in the paper. Data files may be requested from the authors. Requests for materials should be addressed to Y.L. or R.-W.L.

Submitted 18 January 2018
Accepted 6 August 2018
Published 19 September 2018
10.1126/scirobotics.aat0429

Citation: Y. Wu, Y. Liu, Y. Zhou, Q. Man, C. Hu, W. Asghar, F. Li, Z. Yu, J. Shang, G. Liu, M. Liao, R.-W. Li, A skin-inspired tactile sensor for smart prosthetics. *Sci. Robot.* **3**, eaat0429 (2018).

Science Robotics

A skin-inspired tactile sensor for smart prosthetics

Yuanzhao Wu, Yiwei Liu, Youlin Zhou, Qikui Man, Chao Hu, Waqas Asghar, Fali Li, Zhe Yu, Jie Shang, Gang Liu, Meiyong Liao, and Run-Wei Li

Sci. Robot. **3** (22), eaat0429. DOI: 10.1126/scirobotics.aat0429

Science Robotics (ISSN 2470-9476) is published by the American Association for the Advancement of Science. 1200 New York Avenue NW, Washington, DC 20005. The title *Science Robotics* is a registered trademark of AAAS.